Supporting Information

19% efficient and stable organic photovoltaic enabled by guest nonfullerene acceptor with fibril-like morphology

Hu Chen,[ab] Sang Young Jeong,[c] Junfu Tian,[d] Yadong Zhang,[e] Dipti R. Naphade,[b] Maryam Alsufyani,[d] Weimin Zhang,[b] Sophie Griggs,[d] Hanlin Hu,[f] Stephen Barlow,[e] Han Young Woo,[c] Seth R Marder,[e] Thomas D. Anthopoulos,[b] Iain McCulloch,[bd] Yuanbao Lin*[bd]

Experimental details

ITO/SAM Hole-Collecting Electrode Fabrication: The Cl-2PACz and Br-2PACz molecules were synthesized according to the previous literature.[1] The SAM molecules were dissolved in absolute ethanol (WWR Inc.) with a concentration of 0.3 mg/ml and left to stir at room temperature for 1 h. Before using, the SAM solution was placed into an ultrasonic bath for 15 min. Indium tin oxide (ITO) coated glass substrates (Kintec Company, 10 Ω $sq.^{-1}$) were cleaned by sequential ultrasonication in dilute Extran 300 detergent solution, deionized water, acetone and isopropyl alcohol for 10 min each. The clean substrates were then subjected to O_2-plasma treatment step for 10 min. The Cl-2PACz solution (150 μL for 2.5×2.5 cm^2 substrate) was applied directly onto the ITO substrate for 20 s followed by a spin-coating step at 3000 rpm for 30 s. The ITO/SAM substrate was then placed onto a hotplate and annealed at 50 °C for 4 min. Next, the ITO/SAM substrate was dynamically washed 2 times with the same SAM solution (0.3 mg/ml). During the latter step, the ITO/SAM substrate was spun at 6000 rpm first while the SAM solution (150 μL for 2.5×2.5 cm^2 substrates) was drop casted on the spinning substrate. The dynamic washing step was repeated twice. All steps were performed in ambient air. Finally, the ITO/SAM substrates were transferred inside a dry nitrogen glove box for solar cell fabrication.

Solar Cell Fabrication: PNDIT-F3N, PM6, and BTP-eC9 were purchased from Solarmer Materials Inc. A solution of PM6:BTP-eC9:isoIDTIC (ratio 1:0.1:1.1, 18 mg mL^{-1} in chloroform containing 0.5 vol% 1,8-diiodooctane (DIO)) was then spun at

3500 rpm for 30 s to obtain an active-layer thickness around 100 nm. A layer of 5 nm of PNDIT-F3N (0.5 mg/mL in methanol, and added 0.5 vol% acetic acid) was spun on top of the BHJ layer. Finally, the samples were placed in a thermal evaporator and 100 nm of silver was then thermally evaporated at 5×10^{-6} mbar through a 0.1 cm^2 pixel area shadow mask. A shadow mask with aperture area of 0.0784 cm^2 was used for *J-V* measurement.

Density Functional Theory (DFT) calculations: The molecular geometry of isoIDTIC and BTP-eC9 was first energy minimized with molecular dynamics using the MMFF94 force field. The optimized conformation was further optimized with Gaussian09 using B3LYP-D3/6-31G(d,p), which was also used to evaluate the energy of HOMO and LUMO was evaluated.

Device Characterization: UV-vis spectra were recorded on a Cary 5000 instrument in single beam mode. *J-V* measurements of solar cells were performed in an N_2 filled glove box using a Keithley 2400 source meter and SS-X50 Solar Simulator (Enli Technology Co., Ltd.,Taiwan). The shadow mask with aperture area of 0.0784 cm^2 was used for *J-V* measurement. The EQE spectra were measured through the Solar Cell Spectral Response Measurement System QE-R3011 (Enli Technology Co., Ltd.,Taiwan). Bruker atomic force microscope (AFM) was used to image the surface of the various layers in tapping mode. TOF-SIMS measurement (Hiden Analytical Company (Warrington-UK)) operated under vacuum conditions (10^{-9} Torr), typically. A continuous Ar+ beam was employed at 4 keV to sputter the surface while the selected ions were sequentially collected using a MAXIM spectrometer equipped with a

quadrupole analyzer. The raster of the sputtered area is estimated to be 750 × 750 μm^2. The acquisition area from which the depth profiling data are obtained was ≈75 × 75 μm^2. The GIWAXS measurement was carried out at the PLS-II 6A U-SAXS beamline of the Pohang Accelerator Laboratory in Korea. The X-rays coming from the in-vacuum undulator (IVU) were monochromated (wavelength, λ = 1.10994 Å) using a double crystal monochromator and focused both horizontally and vertically (450 (H) × 60 (V) μm^2 in FWHM @ the sample position) using K-B type mirrors. The grazing incidence wide-angle X-ray scattering (GIWAXS) sample stage was equipped with a 7-axis motorized stage for the fine alignment of the sample, and the incidence angles of the X-ray beam were set to be 0.12°-0.16° for the neat and blend films. The GIWAXS patterns were recorded with a 2D CCD detector (Rayonix SX165) and an X-ray irradiation time within 100 s, dependent on the saturation level of the detector.

Light-Intensity Dependence Measurements: Light-intensity dependence measurements were performed with PAIOS instrumentation (Fluxim) (steady-state and transient modes). Transient photo-voltage (TPV) measurements monitor the photovoltage decay upon a small optical perturbation during various constant light-intensity biases and at open-circuit bias conditions. Variable light-intensity bias lead to a range of measured V_{OC} values that were used for the analysis. During the measurements a small optical perturbation (<3% of the V_{OC}, so that $\Delta V_{OC} << V_{OC}$) was applied. The subsequent voltage decay was then recorded to directly monitor bimolecular charge carrier recombination. The photovoltage decay kinetics of all devices follow a mono-exponential decay: $\delta V = A \exp(-t/\tau)$, where t is the time and τ is the charge carrier

lifetime. Photo-CELIV measurements (ramp rate 200 V ms^{-1}, delay time: 0 s, offset voltage: 0 V, light-pulse length: 100 μs) were also performed using PAIOS for different light intensities. The light intensity is given in the maximum power of the LED source (100% ≈ 200 mW cm^{-2}).

Electrochemical Impedance Spectroscopy (EIS): EIS was conducted using a commercially available PAIOS. The measurements were performed under open circuit voltage conditions for the OPV in the dark, and in the frequency range between 300 Hz to 3 MHz.

Synthetic details: Details of the synthesis of isoIDTIC are provided in **Scheme 1**. All reagents from commercial sources were used without further purification. Solvents were dried and purified using standard techniques. All compounds were characterized by ^{1}H NMR, ^{13}C NMR (Figure S2) on a Bruker Avance III Ultrashielded Plus instrument.

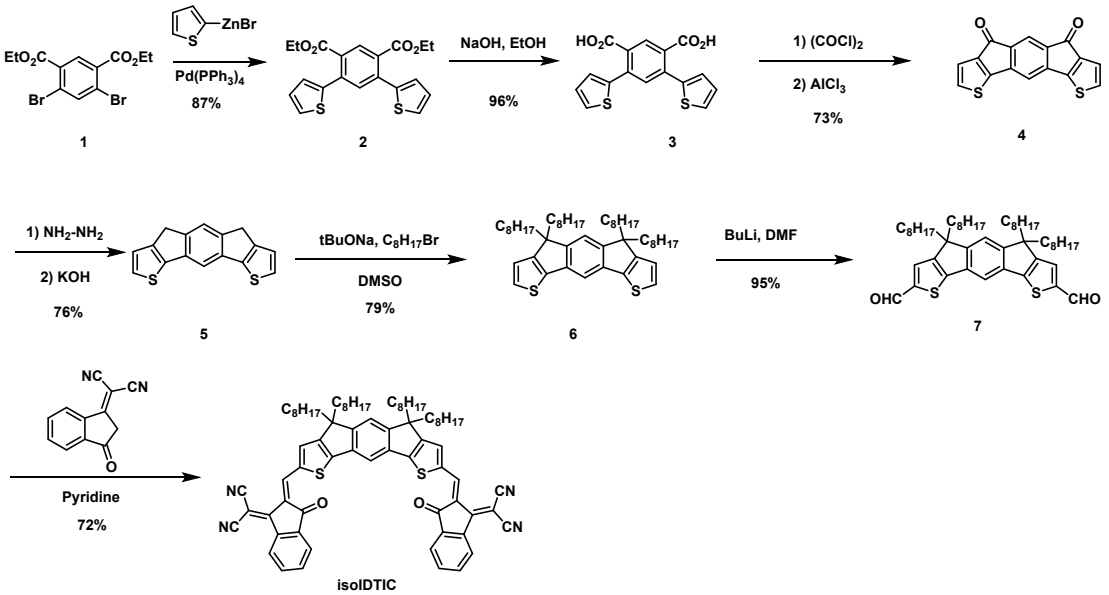

Scheme 1. Synthesis isoIDTIC.

Diethyl 4,6-di(thiophen-2-yl)isophthalate (2)

A mixture of diethyl 4,6-dibromoisophthalate (4.27 g, 11.24 mmol), 2-thienylzinc bromide (0.50 M in THF, 50 mL, 25.0 mmol) and $Pd(PPh_3)_4$ (0.39 g, 0.34 mmol) was heated at reflux for 3 h. After cooled to room temperature, the reaction mixture was poured into sat. NH_4Cl solution. The product was extracted with ethyl acetate (3 × 100 ml). The extracts were combined and washed with water and brine then dried over sodium sulphate. After filtration, the solvent was removed under reduced pressure. The residue was purified by column chromatography on silica, eluting with hexanes/ethyl acetate, to give 2,5-dithien-2-ylterephthalic acid diethyl ester as yellow solid (3.78 g, 87%).

^{1}H NMR (700 MHz, $CDCl_3$): δ 8.16 (s, 1H), 7.62 (s, 1H), 7.41 (d, J = 4.7 Hz, 2H), 7.17 – 7.00 (m, 4H), 4.25 (q, J = 7.2 Hz, 4H), 1.19 (t, J = 7.2 Hz, 6H); ^{13}C {^{1}H} NMR (176 MHz, $CDCl_3$) δ 167.44, 140.53, 136.70, 133.74, 131.12, 130.95, 127.30, 127.16, 126.63, 61.49, 13.81.

4,6-Di(thiophen-2-yl)isophthalic acid (3)

Diethyl 4,6-di(thiophen-2-yl)isophthalate (3.20g, 8.28 mmol) was dissolved in ethanol (200 mL), followed by the addition of a solution of sodium hydroxide (4.50 g NaOH in 30 mL water). This mixture was heated at reflux for 15 h, then evaporated under reduced pressure. Water, and then concentrated hydrochloric acid, was added to the residue. The precipitate formed was collected by filtration and washed with water then dried *in vacuo* to afford product as white solid (2.63 g, 96%).

^{1}H NMR (700 MHz, DMSO-d_6): δ 13.29 (s, 2H), 7.86 (s, 1H), 7.63 (dd, J = 5.1, 1.2 Hz, 2H), 7.50 (s, 1H), 7.24 (dd, J = 3.6, 1.2 Hz, 2H), 7.10 (dd, J = 5.1, 3.5 Hz, 2H); ^{13}C {^{1}H} NNMR (176 MHz, DMSO-d_6): δ 168.65, 139.90, 134.72, 132.13, 131.80, 131.55, 129.62, 127.82, 127.58.

s-Indaceno[1,2-b:7,6-b']dithiophene-4,6-dione (4)

4,6-Di(thiophen-2-yl)isophthalic acid (2.13 g, 6.45 mmol) was suspended in anhydrous DCM (100 mL), followed by the addition of oxalyl chloride (3.28 g, 25.83 mmol). To this mixture anhydrous DMF (1 mL) was added dropwise at room temperature. The resultant mixture was stirred overnight. The solvent was removed under reduced pressure to afford crude acid dichloride as a yellow solid. This solid was dissolved in

anhydrous DCM (80 mL) then added to a suspension of anhydrous AlCl3 (4 g) in DCM (120 mL) at 0 °C. The resultant mixture was allowed to warm to room temperature and stirred overnight, then poured into ice-cold aqueous HCl solution. The precipitate was collected by filtration and washed with 2M HCl solution, water and acetone, then dried *in vacuo* to afford a deep blue solid (1.39 g, 73% if pure). The solubility of the product is too poor to get clear NMR spectra.

4,6-Dihydro-s-indaceno[1,2-b:7,6-b']dithiophene (5)

A mixture of the crude s-indaceno[1,2-b:7,6-b']dithiophene-4,6-dione from the previous reaction (1.33g, 4.52mmol if pure), hydrazine monohydrate (4.52 g, 90.40 mmol) and KOH (5.07 g, 90.54 mmol) in diethylene glycol (50 mL) was heated at 180 ºC for 24 h, then poured into ice containing hydrochloric acid. The precipitate was collected by filtration and washed with water and acetone, and dried *in vacuo* to give 4,6-dihydro-s-indaceno[1,2-b:7,6-b']dithiophene as yellow solid (0.92g, 76%).

^{1}H NMR (700 MHz, $CDCl_3$) δ 7.61 (s, 1H), 7.59 (s, 1H), 7.31 (d, *J* = 4.8 Hz, 2H), 7.12 (d, *J* = 4.8 Hz, 2H), 3.72 (s, 4H); ^{13}C {^{1}H} NMR (176 MHz, $CDCl_3$) δ 147.21, 143.23, 143.21, 137.73, 126.59, 122.70, 122.07, 109.31, 33.80.

4,4,6,6-Tetrahexadecyl-4,6-dihydro-s-indaceno[1,2-b:7,6-b']dithiophene (6)

To a suspension of 4,6-dihydro-s-indaceno[1,2-b:7,6-b']dithiophene (0.92 g, 3.46 mmol) in anhydrous DMSO (20 mL) was added sodium tert-butoxide (1.99 g, 20.73 mmol) in parts. The reaction mixture was heated at 80 ºC for 1 h, followed by the addition of 1-bromooctane (4.00 g, 20.75 mmol) dropwise. After complete addition, the resultant mixture was heated at 85 ºC for 5 h, then poured into ice-water. The precipitate was collected by filtration and washed with water and methanol to give a black solid. This was purified by column chromatography on silica, eluting with hexanes, to give a yellow solid (1,96 g, 79%).

^{1}H NMR (950 MHz, $CDCl_3$) δ7.28 (m, 3H), δ7.16 (s, 1H), 6.96 (d, J = 4.8 Hz, 2H), 2.12 – 2.01 (m, 4H), 2.01 – 1.89 (m, 4H), 1.31 – 1.01 (m, 42H), 0.94-0.73(m, 18H); 13C NMR (239 MHz, $CDCl_3$) δ155.22, 151.29, 141.41, 137.12, 126.50, 121.33, 117.07, 109.10, 53.62, 39.32, 31.83, 30.10, 29.40, 29.30, 24.17, 22.61, 14.06.

4,4,6,6-Tetraoctyl-4,6-dihydro-s-indaceno[1,2-b:7,6-b']dithiophene-2,8-dicarbaldehyde (7)

4,4,6,6-Tetrahexadecyl-4,6-dihydro-s-indaceno[1,2-b:7,6-b']dithiophene (0.67g, 0.94 mmol) was dissolved in anhydrous THF (20 mL) and cooled to -78 ºC, followed by the addition of nBuLi (2.5M, 0.94 mL). The mixture was stirred at -78 ºC for 30 min and then DMF (0.5 mL) was added. The mixture was slowly warmed up to room temperature and stirred overnight. Water (10 mL) was added to the mixture and it was extracted with ether three times. The organic phases were collected, dried over magnesium sulfate, filtered, and concentrated under vacuum. The product was purified by column chromatography on silica gel with hexane/ethyl acetate as eluent to give a yellow solid (0.69g, 95%).

^{1}H NMR (700 MHz, $CDCl_3$) δ 9.94 (s, 2H), 7.74 (s, 1H), 7.67 (s, 2H), 7.30 (s, 1H), 2.12 – 2.01 (m, 4H), 2.01 – 1.89 (m, 4H), 1.31 – 1.01 (m, 42H), 0.94-0.73(m, 18H); ^{13}C NMR{^{1}H} (176 MHz, CD_2Cl_2) δ 159.98, 132.50, 132.32, 128.12, 122.62, 113.29, 106.97, 94.60, 89.64, 31.34, 16.15, 8.77, 6.95, 6.34, 6.21, 1.27, -0.42.

2,2'-((2Z,2'Z)-((4,4,6,6-Tetraoctyl-4,6-dihydro-s-indaceno[1,2-b:7,6-b']dithiophene-2,8-diyl)bis(methaneylylidene))bis(3-oxo-2,3-dihydro-1H-indene-2,1-diylidene))dimalononitrile (isoIDTIC)

4,4,6,6-Tetraoctyl-4,6-dihydro-s-indaceno[1,2-b:7,6-b']dithiophene-2,8-dicarbaldehyde (0.72g, 0.94 mmol) was dissolved in pyridine (20 mL), followed by the addition of 2-(3-oxo-2,3-dihydro-1H-inden-1-ylidene)malononitrile (0.46g, 2.35mmol), the mixture was heated to 80 ºC overnight, then diluted with saturated aqueous NH_4Cl, extracted with EtOAc, washed with brine and concentrated in vacuo. The residue was purified by column chromatography on silica gel to provide the title compound as a golden solid (0.76g, 72%).

^{1}H NMR (500 MHz, $CDCl_3$) δ 8.99 (s, 2H), 8.72 (dd, *J* = 6.7, 2.0 Hz, 2H), 8.01 – 7.95 (m, 2H), 7.88 (s, 1H), 7.81 – 7.75 (m, 6H), 7.33 (s, 1H), 2.07 (ddd, *J* = 16.5, 12.1, 4.7 Hz, 4H), 2.01 – 1.93 (m, 4H), 1.27 – 0.96 (m, 40H), 0.81 (t, *J* = 7.1 Hz, 20H). ^{13}C {^{1}H} NMR (126 MHz, $CDCl_3$) δ 188.42, 160.91, 160.12, 158.13, 156.64, 140.95, 140.10, 138.89, 137.84, 137.12, 137.07, 135.22, 134.65, 125.47, 123.97, 122.16, 118.22, 114.94, 114.88, 114.07, 54.64, 39.50, 31.91, 30.08, 29.50, 29.38, 24.54, 22.73, 14.19.

Table S1. Summarized parameters of ternary BHJ OPV devices with PCEs over 18%.

Host Materials	Guest Material	Weight ratio	V_{oc} [V]	J_{sc} [mA cm^{-2}]	FF [%]	PCE$_T$ [%][a]	PCE$_G$ [%][b]	Ref.
PM6:BTP-eC9	isoIDTIC	1:1.1:0.1	0.866	27.3	80.4	19.0	1.7	This work
PM6:L8-BO	D18	0.8:1.2:0.2	0.896	26.7	81.9	19.6	17.7	[2]
PM1:L8-BO	BTP-2F2Cl	1:1.05:0.15	0.881	27.2	80.1	19.2	18.4	[3]
PTQ10:BTP-FTh	IDIC	1:08:0.2	0.870	27.2	80.6	19.1	12.4	[4]
PBQx-TF:BTPeC9-2Cl	F-BTA3	1:1:0.2	0.879	26.7	80.9	19.0	12.5	[5]
PM6:BTP-eC9	HDO-4Cl	1:1:0.2	0.866	27.1	80.5	18.9	15.4	[6]
PM6:BTP-eC9	BTP-sC9	1:0.6:0.6	0.861	27.5	79.3	18.8	17.5	[7]
PM6:BTP-eC9	L8-BO-F	1:1.05:0.15	0.853	27.4	80.0	18.7	16.9	[8]
PM6:BTP-eC9	PB2F	0.8:1.2:0.2	0.863	26.8	80.4	18.6	5.2	[9]
PM6:BTP-eC9	PM6-Si30	0.85:0.15:1.2	0.870	26.9	78.0	18.3	14.3	[10]
PM6:BO-4Cl	BTP-S2	1:0.95:0.25	0.861	27.1	78.0	18.2	15.1	[11]
PM6:Y6	ITIC-M	1:1.15:0.05	0.859	26.4	80.1	18.1	8.8	[12]
PM6:Y6	AQx-3	1:0.8:0.4	0.870	26.8	77.2	18.0	16.7	[13]

[a]The PCEs of ternary BHJ devices.

[b]The PCEs of guest binary BHJ devices.

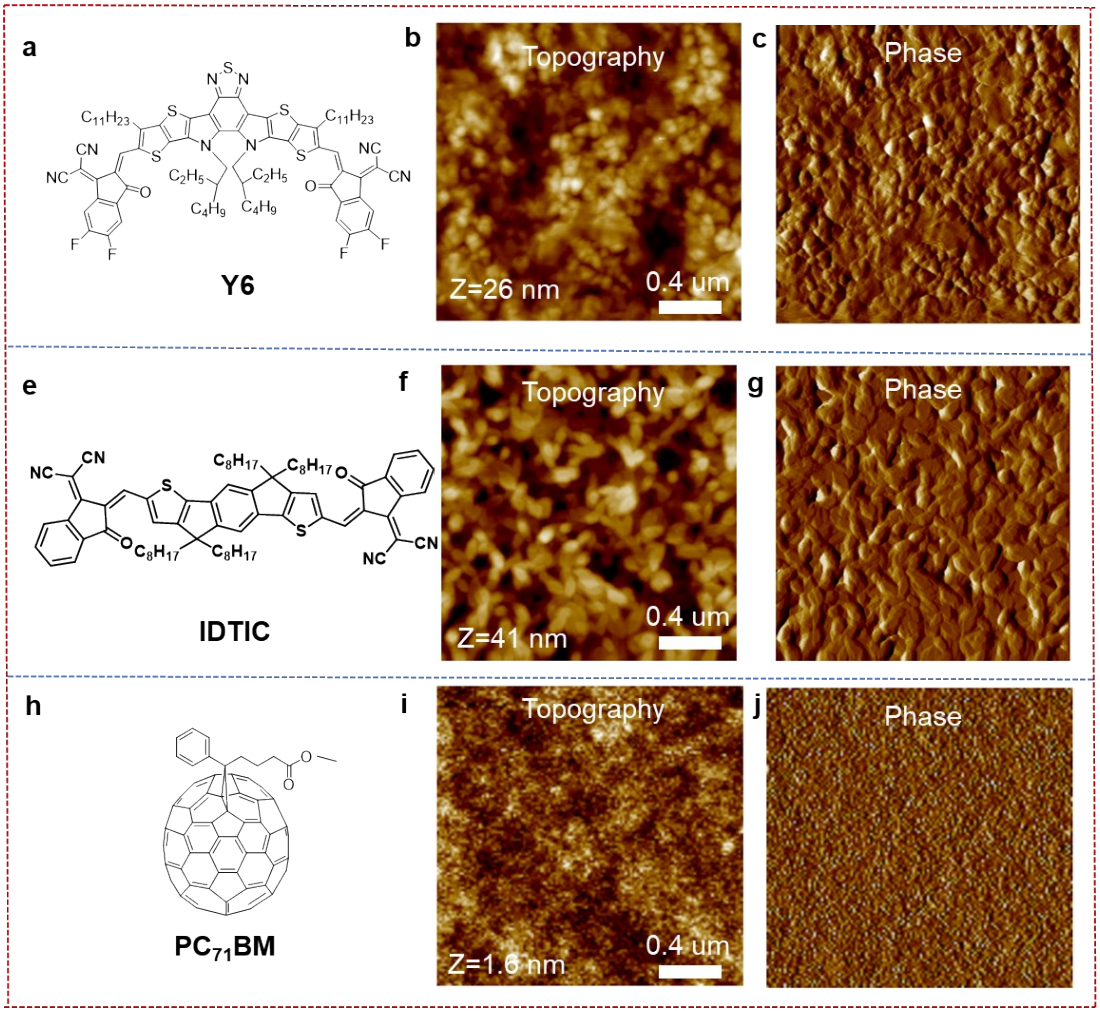

Fig. S1. Chemical structures, AFM height, and phase images of Y6, IDTIC, and $PC_{71}BM$.

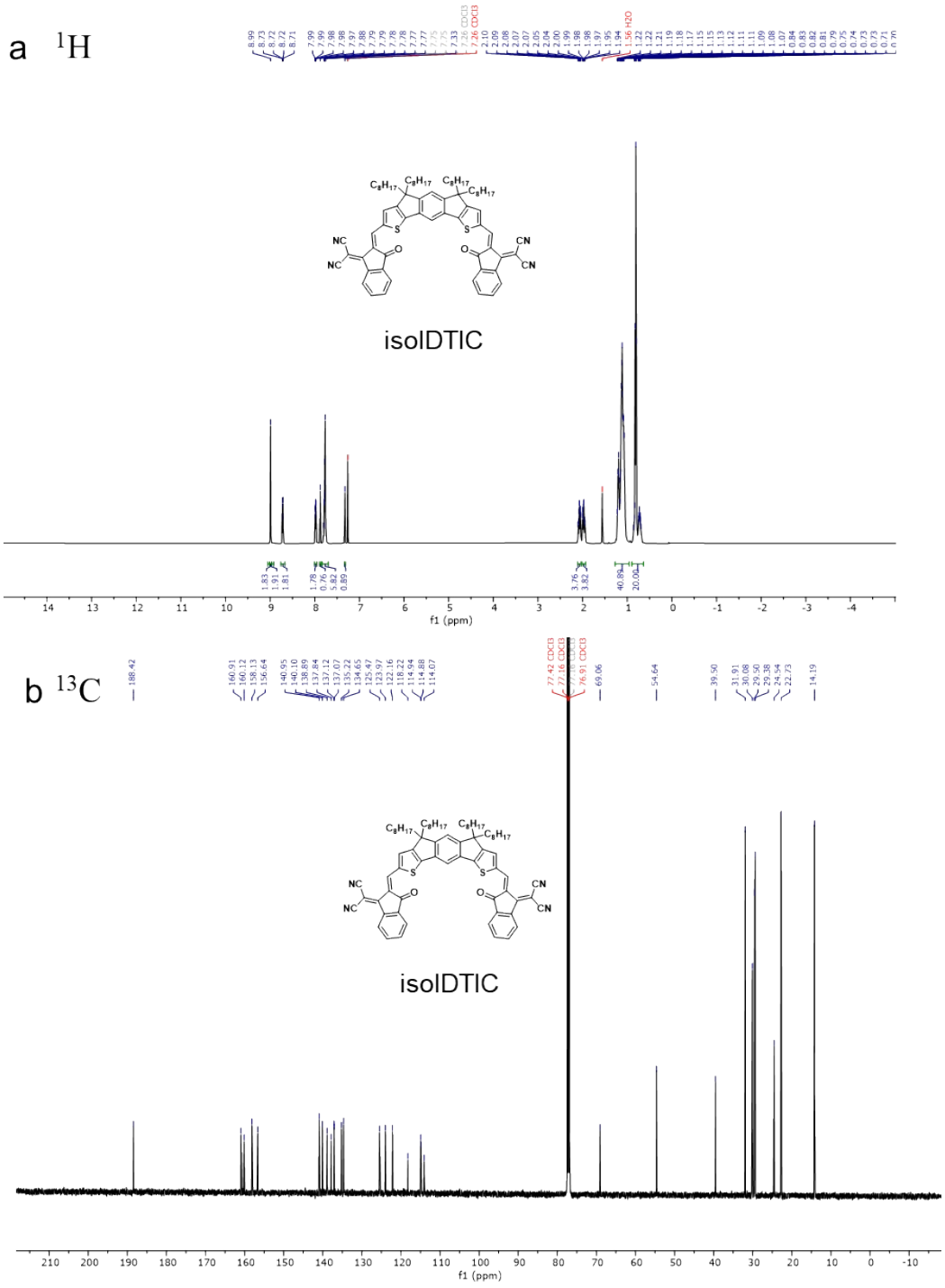

Fig. S2. (a) ^{1}H NMR spectrum and (b) ^{13}C {^{1}H} NMR spectrum of isoIDTIC in $CDCl_3$.

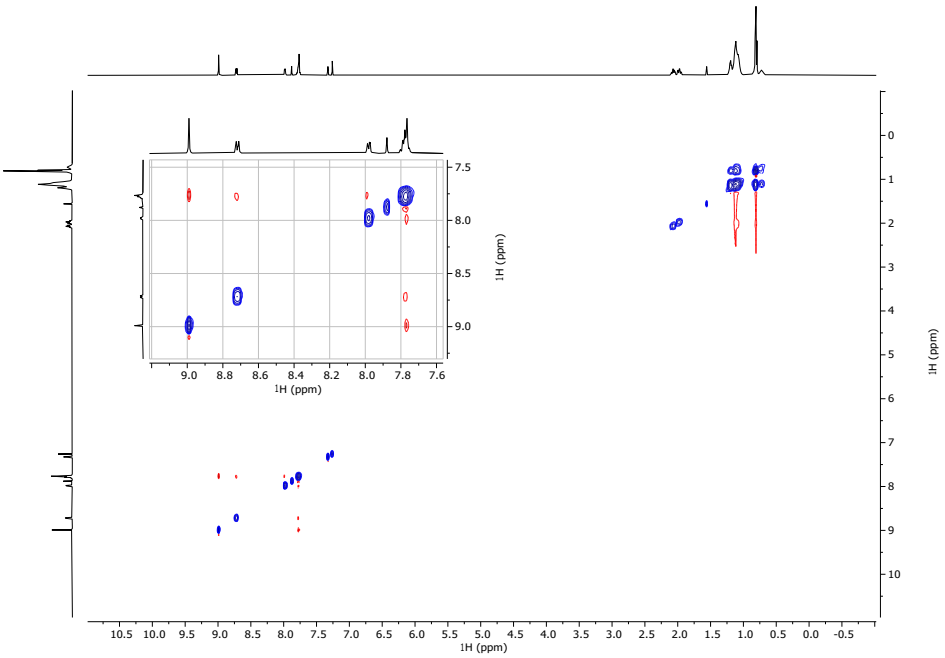

Fig. S3. 2D ROESY of isoIDTIC in $CDCl_3$.

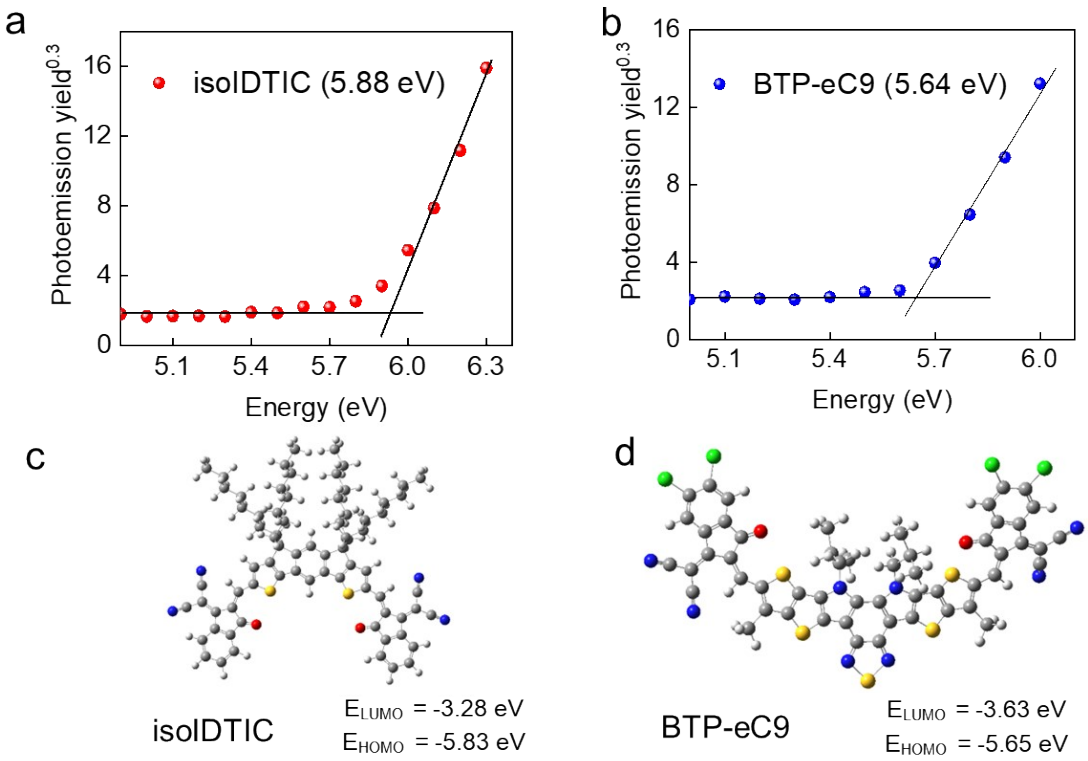

Fig. S4. Photoelectron spectroscopy in air (PESA) measurement of (a) isoIDTIC, and (b) BTP-eC9. The DFT calculations of (c) isoIDTIC, and (d) BTP-eC9.

Table S2. The summarized parameters of isoIDTIC and BTP-eC9 acceptors.

Materials	λ_{max} (nm)	E_{gap}^{opt} (eV)	$HOMO_{exp}$ (eV)	$LUMO_{exp}$ (eV)	$HOMO_{cal}$ (eV)	$LUMO_{cal}$ (eV)
isoIDTIC	608	1.90	-5.86	-3.96	-5.83	-3.28
BTP-eC9	830	1.57	-5.64	-4.07	-5.65	-3.63

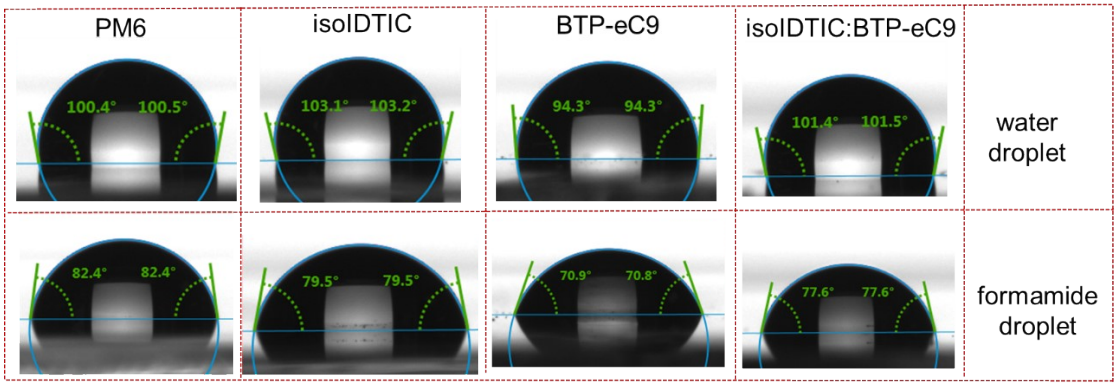

Fig. S5. Photographs of water (top row) and formamide (bottom row) droplets in contact with the various layer surfaces.

Table S3. Contact angles, surface energy on various neat films.

Solid surface	Water contact angle	Formamide contact angle	Surface energy (γ) [mN/m][a]
PM6	100.0 ±1.1˚	82.3±0.7˚	20.3
isoIDTIC	103.0±1.3˚	79.6±0.6˚	25.6
BTP-eC9	94.5±1.1˚	71.0±0.6˚	29.4
isoIDTIC:BTP-eC9	101.2±1.3˚	77.5±0.8˚	26.5

[a]Surface energy was converted from contact angle values based on the Owens, Wendt, Rabel, and Kaelble (OWRK) equation method.

Table S4. Flory-Huggins parameter and interfacial tension of different blends.

Blend (A:B)	Flory-Huggins Parameter ($\chi_{A:B}$)	Interfacial Tension (γ_{AB})
PM6:BTP-eC9	0.84	1.30 mN/m
PM6:isoIDTIC	0.30	0.45 mN/m
BTP-eC9:isoIDTIC	0.13	0.22 mN/m

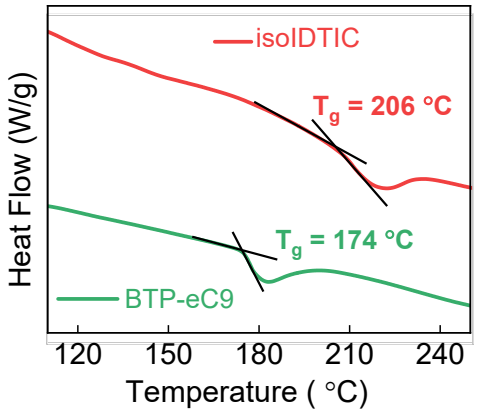

Fig. S6. DSC of isoIDTIC and BTP-eC9 powder.

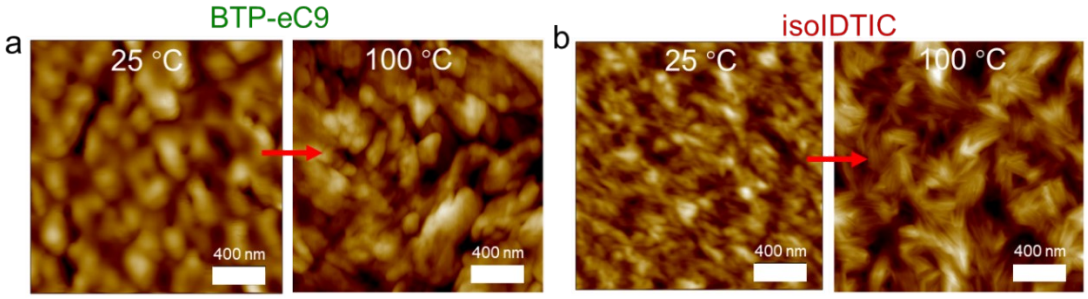

Fig. S7. The AFM topography of (a) BTP-eC9 and (b) isoIDTIC solid films without and with annealing treatment (100 °C at 10 mins) .

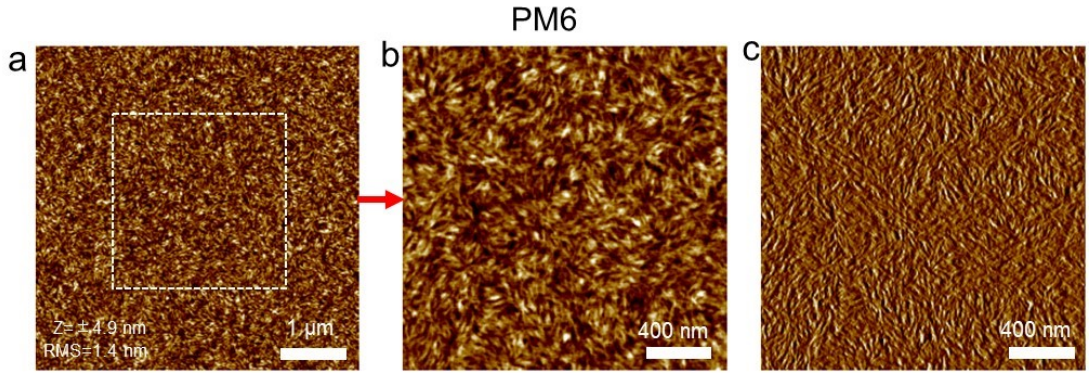

Fig. S8. (a) The AFM topography of PM6 solid film, while (b) and (c) are the high-resolution AFM height and phase images corresponding to the white frame in (a).

Table S5. Ordered molecular structure parameters of the blend BHJ films, obtained from GIWAXS.

Film	Lamellar stacking				π-π stacking			
	Location [Å^{-1}]	d_L [Å]	FWHM [Å^{-1}]	CCL[a] [Å]	Location [Å^{-1}]	dπ [Å]	FWHM [Å^{-1}]	CCL [Å]
PM6:BTP-	0.30	20.94	0.076	74.40	1.71	3.67	0.268	21.10

eC9 PM6:BTP-eC9:isoIDTIC	0.29	21.67	0.066	85.68	1.71	3.67	0.237	23.86

[a]Crystal coherence length (CCL) was calculated according to Scherrer equation CCL = 2πK/Δq, where K is the shape factor (K = 0.9) and Δq is the full width at half-maximum (FWHM) of diffraction peak

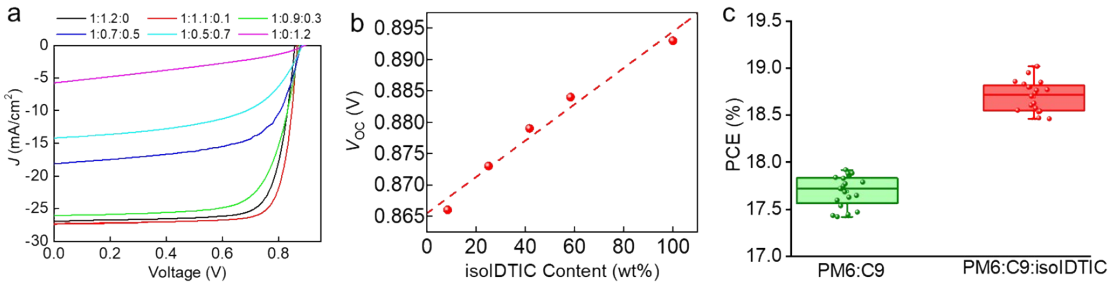

Fig. S9. (a) *J-V* curves of ternary devices with different isoIDTIC contents. (b) The *V*oc of OPVs device with different isoIDTIC contents. (c) The box charts of PCEs of the OPV with PM6:BTP-eC9 (green) and PM6:BTP-eC9:isoIDTCI (red).

Table S6. Photovoltaic parameters of OPVs, measured under the illumination of AM 1.5 G at 100 mW/cm^2.

PM6:BTP-eC9:isoIDTIC	V_{OC} [V]	J_{SC} [mA/cm^2]	FF [%]	PCE [%][a]
1:1.2:0	0.857	26.95	77.5	17.9 (17.7±0.2)
1:1.1:0.1	0.866	27.30	80.4	19.0 (18.7±0.2)
1:0.9:0.3	0.873	26.07	71.1	16.2 (15.7±0.3)
1:0.7:0.5	0.879	18.13	62.9	10.0 (9.5±0.3)
1:0.5:0.7	0.884	14.20	54.9	6.9 (6.3±0.5)
1:0:1.2	0.893	5.75	32.3	1.7 (1.5±0.2)

[a] The values in bracket are average PCE values obtained from 20 different cells.

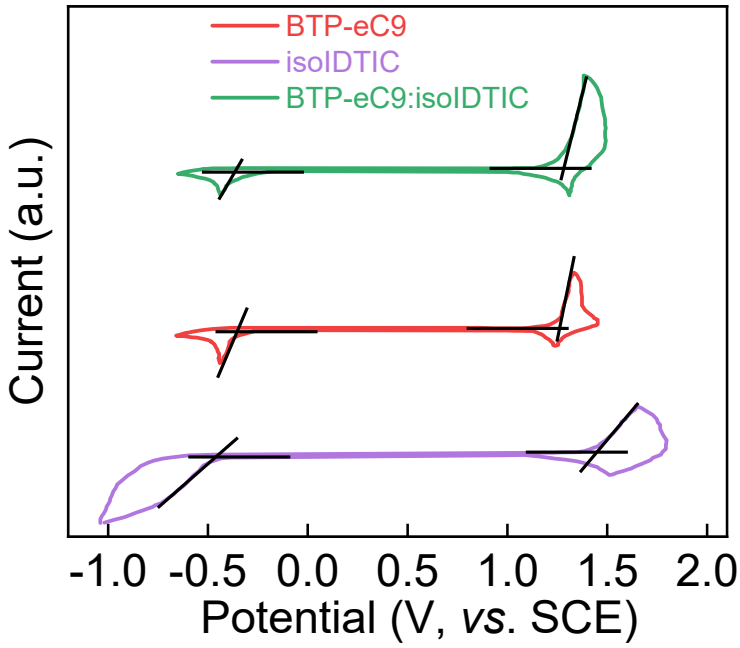

Fig. S10. Cyclic voltammograms of BTP-eC9, isoIDTIC, and BTP-eC9:isoIDTIC (1.1:0.1, wt%). The HOMO and LUMO positions are determined by the point of intersection using two tangent lines at the onsets of oxidation or reduction waves. The equation of $E_{LUMO/HOMO}$ = -e($E_{red/ox}$+4.41) (eV) was used to calculate the LUMO and HOMO levels (the redox potential of Fc/Fc^+ is found to be 0.39 V).

Table S7. The HOMO and LUMO of BTP-eC9, isoIDTIC, and BTP-eC9:isoIDTIC (1.1:0.1, wt%) calculated by cyclic voltammograms.

Compound	HOMO [eV]	LUMO [eV]
BTP-eC9	-5.67	-4.05
isoIDTIC	-5.86	-3.96
BTP-eC9:isoIDTIC	-5.69	-4.04

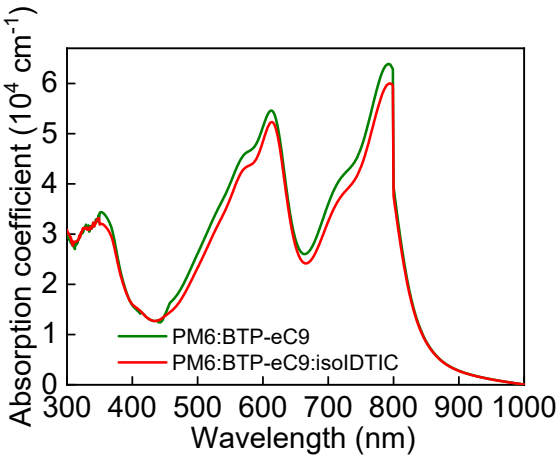

Fig. S11. UV-Vis absorption coefficient of PM6:BTP-eC9 and PM6:BTP-eC9:isoIDTIC films.

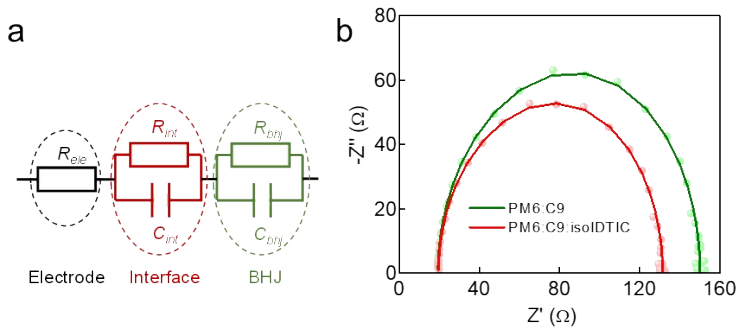

Fig. S12. (a) The equivalent-circuit model employed for EIS fitting and (b) Nyquist plots of the OPV devices. R_{ele} corresponds to electrode resistance including ITO and Ag; R_{int} and C_{int} parallel connection corresponds to resistance and capacitance of the interface layer; R_{bhj} and C_{bhj} parallel connection corresponds to resistance and capacitance of the BHJ layer.

Table S8. Fitting parameters for OPVs from Nyquist plots.

BHJ	R_{ele} [Ω]	R_{int} [Ω]	C_{int} [nF]	R_{bhj} [Ω]	C_{bhj} [nF]
PM6:C9	19.4	25.7	34.1	105.2	20.5
PM6:C9:isoIDTIC	19.6	26.9	36.6	85.1	28.6

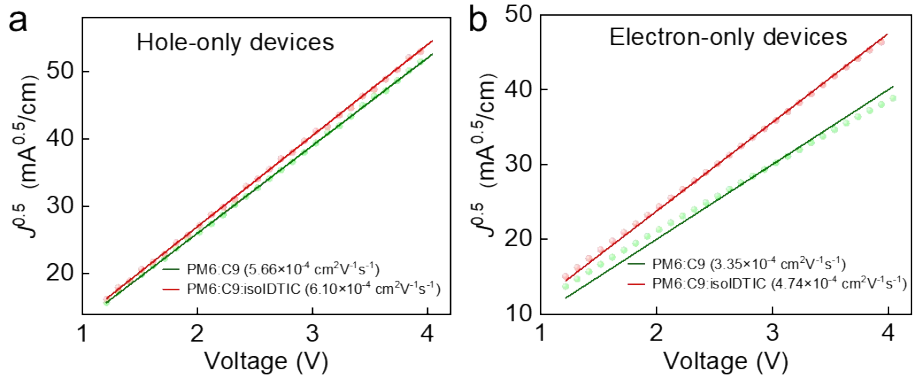

Fig. S13. SCLC of (a) hole-only and (b) electron-only devices with PM6:BTP-eC9 and PM6:BTP-eC9:isoIDTIC BHJ.

Table S9. Fitting parameters for hole and electron mobilities of BHJ films from SCLC.

BHJ	μ_h [cm^2 V^{-1}s^{-1}]	μ_e [cm^2 V^{-1}s^{-1}]	μ_e/μ_h

PM6:BTP-eC9	5.66 (5.1±0.5) ×10^{-4}	3.35 (3.1±0.2) ×10^{-4}	1.69
PM6:BTP-eC9:isoIDTIC	6.10 (5.6±0.4) ×10^{-4}	4.74 (4.3±0.3) ×10^{-4}	1.29

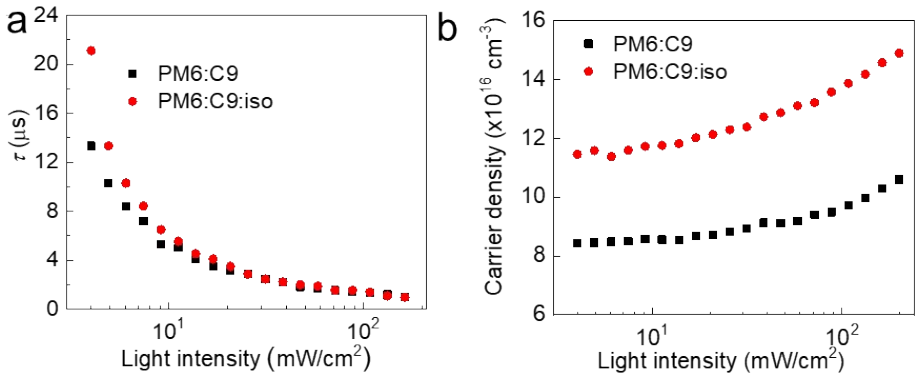

Fig. S14. Light intensity dependence of (a) charge carrier lifetime, and (b) carrier density measured for the OPV devices with PM6:BTP-eC9 and PM6:BTP-eC9:isoIDTIC BHJ.

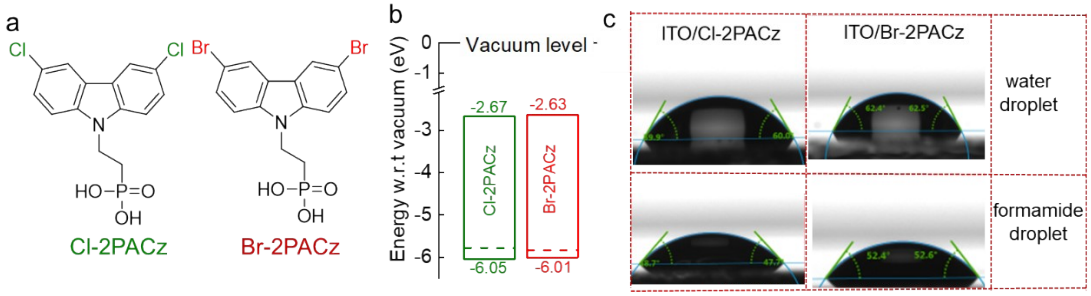

Fig. S15. (a) Chemical structures, (b) energy levels, and (c) contact angles of Cl-2PACz and Br-2PACz SAMs.

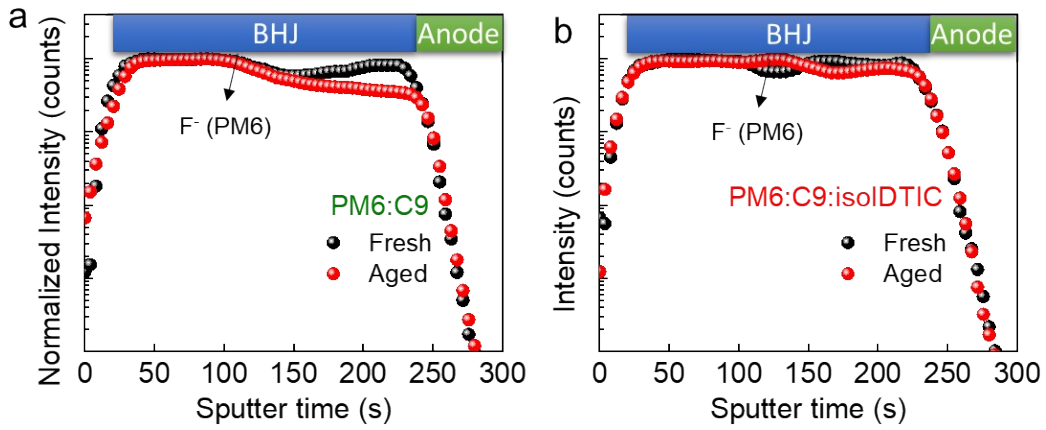

Fig. S16. Normalized ToF-SIMS intensity of F^- against sputtering time.

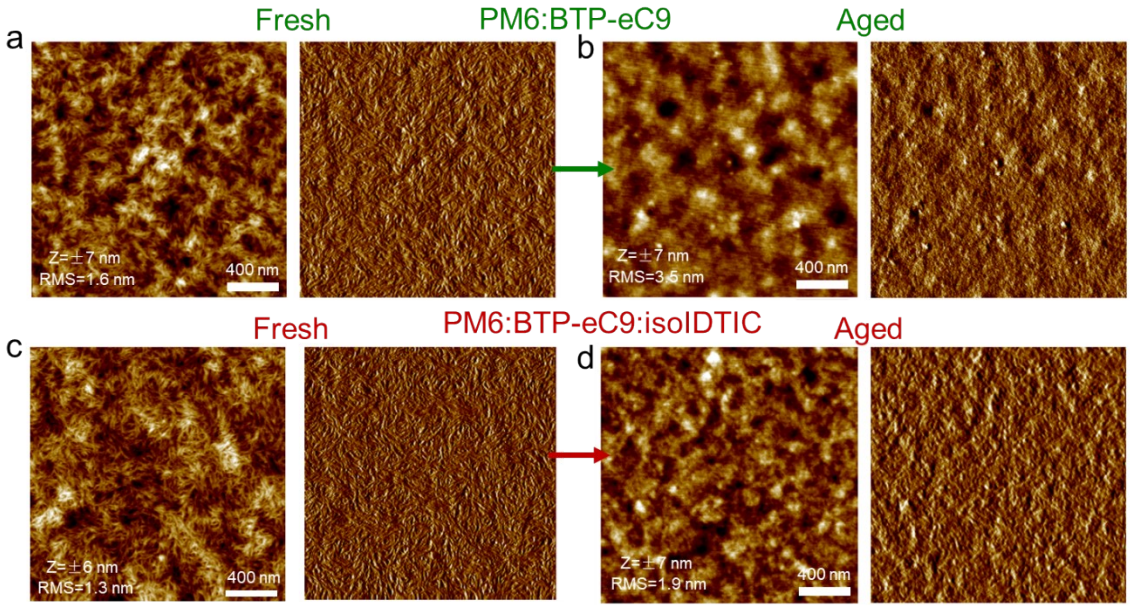

Fig. S17. The AFM topography and phase image of (a) fresh and (b) aged PM6:BTP-eC9 solid films. The AFM topography and phase image of (c) fresh and (d) aged PM6:BTP-eC9:isoIDTIC solid films.

References

1. Y. Lin, Y. Zhang, J. Zhang, M. Marcinskas, T. Malinauskas, A. Magomedov, M. I. Nugraha, D. Kaltsas, D. R. Naphade, G. T. Harrison, A. El-Labban, S. Barlow, S. De Wolf, E. Wang, I. McCulloch, L. Tsetseris, V. Getautis, S. R. Marder and T. D. Anthopoulos, *Adv. Energy Mater.* **2022**, 12, 2202503.
2. L. Zhu, M. Zhang, J. Xu, C. Li, J. Yan, G. Zhou, W. Zhong, T. Hao, J. Song, X. Xue, Z. Zhou, R. Zeng, H. Zhu, C.-C. Chen, R. C. I. MacKenzie, Y. Zou, J. Nelson, Y. Zhang, Y. Sun and F. Liu, *Nat. Mater.* **2022**, 21, 656.
3. R. Sun, Y. Wu, X. Yang, Y. Gao, Z. Chen, K. Li, J. Qiao, T. Wang, J. Guo, C. Liu, X. Hao, H. Zhu and J. Min, *Adv. Mater.* **2022**, 2110147.
4. K. Chong, X. Xu, H. Meng, J. Xue, L. Yu, W. Ma and Q. Peng, *Adv. Mater.* **2022**, 34, 2109516.
5. Y. Cui, Y. Xu, H. Yao, P. Bi, L. Hong, J. Zhang, Y. Zu, T. Zhang, J. Qin, J. Ren, Z. Chen, C. He, X. Hao, Z. Wei and J. Hou, *Adv. Mater.*, 2021, **33**, 2102420.
6. P. Bi, S. Zhang, Z. Chen, Y. Xu, Y. Cui, T. Zhang, J. Ren, J. Qin, L. Hong, X. Hao and J. Hou, *Joule*, 2021, **5**, 2408.
7. L. Zhan, S. Li, Y. Li, R. Sun, J. Min, Z. Bi, W. Ma, Z. Chen, G. Zhou, H. Zhu, M. Shi, L. Zuo and H. Chen, *Joule*, 2022, **6**, 662-675.
8. Y. Cai, Y. Li, R. Wang, H. Wu, Z. Chen, J. Zhang, Z. Ma, X. Hao, Y. Zhao, C. Zhang, F. Huang and Y. Sun, *Adv. Mater.*, 2021, **33**, 2101733.
9. T. Zhang, C. An, P. Bi, Q. Lv, J. Qin, L. Hong, Y. Cui, S. Zhang and J. Hou, *Adv. Energy Mater.*, 2021, **11**, 2101705.
10. W. Peng, Y. Lin, S. Y. Jeong, Z. Genene, A. Magomedov, H. Y. Woo, C. Chen,

W. Wahyudi, Q. Tao, J. Deng, Y. Han, V. Getautis, W. Zhu, T. D. Anthopoulos and E. Wang, *Nano Energy*, 2022, **92**, 106681.
11. L. Zhan, S. Li, X. Xia, Y. Li, X. Lu, L. Zuo, M. Shi and H. Chen, *Adv Mater*, 2021, **33**, 2007231.
12. Y. Zeng, D. Li, H. Wu, Z. Chen, S. Leng, T. Hao, S. Xiong, Q. Xue, Z. Ma, H. Zhu and Q. Bao, *Adv. Funct. Mater.*, 2021, **32**, 2110743.
13. F. Liu, L. Zhou, W. Liu, Z. Zhou, Q. Yue, W. Zheng, R. Sun, W. Liu, S. Xu, H. Fan, L. Feng, Y. Yi, W. Zhang and X. Zhu, *Adv. Mater.*, 2021, **33**, 2100830.